Taylor & Francis
Taylor & Francis Group

Phase Transitions
A Multinational Journal

ISSN: 0141-1594 (Print) 1029-0338 (Online) Journal homepage: https://www.tandfonline.com/loi/gpht20

The nature of the intermediate phase in $K_3Na(SeO_4)_2$ crystals: three possible transition paths of the trigonal-monoclinic phase transition

Yu. E. Kitaev, E. M. Roginskii & V. S. Zhandun

To cite this article: Yu. E. Kitaev, E. M. Roginskii & V. S. Zhandun (2018) The nature of the intermediate phase in $K_3Na(SeO_4)_2$ crystals: three possible transition paths of the trigonal-monoclinic phase transition, Phase Transitions, 91:11, 1135-1146, DOI: 10.1080/01411594.2018.1498497

To link to this article: https://doi.org/10.1080/01411594.2018.1498497

PHASE TRANSITIONS
2018, VOL. 91, NO. 11, 1135–1146
https://doi.org/10.1080/01411594.2018.1498497

Taylor & Francis
Taylor & Francis Group

The nature of the intermediate phase in $K_3Na(SeO_4)_2$ crystals: three possible transition paths of the trigonal-monoclinic phase transition

Yu. E. Kitaev [a], E. M. Roginskii [a] and V. S. Zhandun [b]

[a]Ioffe Institute, St. Petersburg, Russia; [b]Kirensky Institute of Physics, Krasnoyarsk, Russia

ABSTRACT

Three different transition paths of the phase transition from the high-symmetry trigonal $P\bar{3}m1$ to the low-symmetry monoclinic phase $C2/c$ in $K_3Na(SeO_4)_2$ crystals have been analyzed using *ab initio* calculations based on the density functional theory (DFT) as well as programs and retrieval tools of the Bilbao Crystallographic server (BCS). We conclude that the intermediate state observed in experiments within 346–329 K temperature range consists of a mixture of two monoclinic phases $C2/m$ and $C2/c$, both with the primitive cell doubled along the z-axis. Both monoclinic phases result from the softening of the double-degenerated zone-edge soft phonon A_3^+.

ARTICLE HISTORY
Received 11 April 2018
Accepted 2 July 2018

KEYWORDS
Phase transition; glaserite crystals; ab initio; soft modes

1. Introduction

$K_3Na(SeO_4)_2$ crystals belong to the most studied systems of the glaserite crystal family [1–6]. They were investigated by various experimental techniques: X-ray [1], macroscopic measurements (thermal, elastic, and dielectric) [2,3], Raman [4], infrared [5] and nuclear magnetic resonance [6] studies. It was firmly established by X-ray studies [1] that the crystal structures of high-symmetry (high-temperature) and low-symmetry (low-temperature) phases of $K_3Na(SeO_4)_2$ belong to trigonal and monoclinic symmetry respectively. The high-symmetry phase $P\bar{3}m1$ (No. 164) was observed for temperatures higher than 346 K. Calorimetric investigations have shown the existence of a sequence of phase transitions [3]. A clear specific heat anomaly was observed at 346 K as a result of the structural phase transition, whereas a weak anomaly at 329 K proves that additional structural changes appear at this temperature. The structure of the phase below 329 K has been established to have low monoclinic symmetry $C2/c$ (No. 15). The corresponding space groups, lattice parameters and Wyckoff positions of atoms within unit cells determined in [1] are listed below (see Section 3, Table 1). It was also firmly established [1–6] that the phase transition from the high-temperature trigonal phase to the low-temperature monoclinic phase $C2/c$ (No. 15) goes *via* an intermediate phase observed within the temperature interval 346–329 K. However, the symmetry of the intermediate phase is still remained controversial. The authors of [3] conclude that the intermediate phase is $B2/m$ whereas the $P\bar{3}c1$ intermediate phase was proposed in [2]. The intermediate monoclinic $C2/m$ phase in another compound of the glaserite family, namely $K_3Na(CrO_4)_2$ has been found in [7–9].

For the study of phase transitions in $K_3Na(SeO_4)_2$ crystals, we will apply a combination of *ab initio* calculations of phonon spectra and group theoretical approach based on the programs and retrieval tools of the Bilbao Crystallographic server [10–12].

CONTACT Yu. E. Kitaev yu.kitaev@mail.ru

Table 1. Experimental structure data [1] of trigonal and monoclinic phases of $K_3Na(SeO_4)_2$.

Trigonal phase				Monoclinic phase*			
Space group *P$\bar{3}$m1 (No. 164)*				Space group *C2/c (No.15)*			
$a = 5.906$ Å				$a = 10.162$ Å			
$b = 5.906$ Å				$b = 5.867$ Å			
$c = 7.5552$ Å				$c = 15.021$			
$\alpha = 90°$				$\alpha = 90°$			
$\beta = 90°$				$\beta = 90°$			
$\gamma = 120°$				$\gamma = 90°$			
Na 1a	0.000000	0.000000	0.000000	Na 4a	0.000000	0.000000	0.000000
K 1b	0.000000	0.000000	0.500000	K 4e	0.000000	0.973300	0.250000
K 2d	0.333333	0.666667	0.824000	K 8f	0.168100	0.488880	0.412930
Se 2d	0.333333	0.666667	0.272440	Se 8f	0.165660	0.492420	0.136750
O 2d	0.333333	0.666667	0.485200	O 8f	0.170900	0.527500	0.243400
O 6i	0.184200	0.368400	0.196500	O 8f	0.090300	0.707400	0.089400
				O 8f	0.089600	0.258000	0.108600
				O 8f	0.315100	0.481900	0.096600

*The low-symmetry structure corresponds to the space group setting with the unique axis **b**.

2. *Ab initio* calculations: computational details

The calculations were carried out with VASP code [13,14] using the plane-wave basis set for valence electronic states. Exchange and correlation were treated within the Generalized Gradient Approximation (GGA) approximation to DFT with the Perdew-Burke-Ernzerhof (PBE) exchange-correlation functional [15]. The projector-augmented wave (PAW) method [16,17] was used to describe the interactions between the core and valence electrons. The 2p3s states of the Na atom, 3s3p4s of the K atom and 4s4p of the Se atom while 2s2p states of the O atom were considered as valence states. To calculate the equilibrium lattice parameters, optimizations of the $K_3Na(SeO_4)_2$ structure were performed for a series of five volumes of the unit cell. In each case, the atomic positions and cell parameters were allowed to relax, whereas the volume and the symmetry of the lattice were kept fixed. The structural optimization was deemed to be converged when the maximum force on ions was lower than 2×10^{-3} eV Å^{-1}. The resulting energy *versus* volume curve was fitted by the Murnaghan equation of state [18] to obtain the equilibrium cell volume. This approach avoided the problems related to the Pulay stress and the changes of the plane-wave basis-set size that accompany volume variations. The results were checked for convergence with respect to k-point sampling and plane-waves kinetic energy cutoff. It was found that convergence of the size of plane-wave basis is achieved with the energy cutoff of 950 eV and with a $6 \times 6 \times 6$ grid of k-points chosen according to the Monkhorst-Pack scheme [19] in the irreducible part of the Brillouin zone (BZ). Kohn–Sham equations are solved iteratively to self-consistency within 10^{-8} eV. The minimum energy lattice parameters thus determined were employed in all subsequent calculations that were performed using the same calculation parameters and with the same convergence criterion. The phonon spectrum in the Γ point of the BZ was computed using the density functional perturbation theory (DFPT) approach [13,14]. The phonon band structure was obtained within the supercell approach (we use $2 \times 2 \times 2$ supercell) with the dynamical matrix calculated from the finite displacement method [20,21].

3. Group theoretical analysis

Our theory analysis was based on experimental structure data of $K_3Na(SeO_4)_2$ crystals determined in [1] and summarized in Table 1.

The crystallographic unit cells of trigonal (*P$\bar{3}$m1)* and monoclinic (*C2/c)* phases are presented in Figures 1 and 2, respectively.

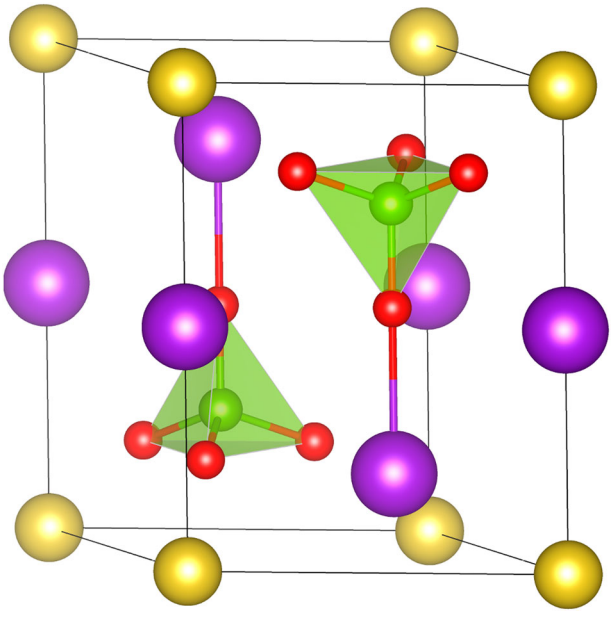

Figure 1. (color online) Crystal structure of the trigonal ($P\bar{3}m1$) phase of $K_3Na(SeO_4)_2$. Large (dark violet) filled atoms are the potassium ones, opened (yellow) atoms are the sodium ones, oxygen atoms are at the corners of tetrahedrae with selenium atoms at the tetrahedrae centers.

The phonon symmetries in high-temperature and low-temperature phases determined by the SITESYM program [10–12] are presented in Tables 2 and 3, respectively.

In Tables 2 and 3, the irreducible representations (irreps) of the space groups describing the symmetry of phonons at the BZ symmetry points are generated by the irreps β of the groups of sites $\boldsymbol{q}$ where the atoms given in columns 1 are located. The localized atomic displacements x, y, and z are transformed according to these site-group irreps. The space group irreps are labeled according to [22] and the labeling of the site-group irreps follows [23].

From Tables 2 and 3 one can write down the vibrational representation at any point of the BZs summarizing the contributions of all the atoms in the primitive unit cell. For example, in the high-symmetry trigonal phase (space group $P\bar{3}m1$), the local z-displacements of K2 atoms transforming according to the $a_{2u}(z)$ irrep of the site symmetry group $\bar{3}m$ of the Wyckoff position 1b induce at the Γ-point of the BZ the phonon mode 2^- (Γ_2^-), at the A-point the phonon mode 1^+ (A_1^+), at the K-point the phonon mode 2 (K_2) etc.

Thus, the vibrational representation at the Γ-point of the BZ of the trigonal phase is

$$\begin{aligned}\Gamma_{\text{opt}} + \Gamma_{\text{ac}} &= 5\Gamma_1^+ + \Gamma_1^- + \Gamma_2^+ + 7\Gamma_2^- + 6\Gamma_3^+ + 8\Gamma_3^- = 5A_{1g} + A_{1u} + A_{2g} + 7A_{2u} \\ &\quad + 6E_g + 8E_u, \qquad \Gamma_{\text{ac}} = \Gamma_2^- + \Gamma_3^- = A_{2u} + E_u,\end{aligned} \tag{1}$$

with A_{1g} and E_g modes being active in Raman spectra while A_{2u} and E_u modes being active in infrared spectra. The modes A_{1u} and A_{2g} are silent modes forbidden both in Raman and IR spectra by selection rules. The non-zero Raman tensor components for A_{1g} modes are the diagonal elements α_{xx}, α_{yy}, α_{zz}, while for two-dimensional E_g modes are α_{xx}, α_{yy}, α_{xy}, α_{yz}.

Similarly, the set of phonon modes at the A-point of the BZ is

$$A = 6A_1^+ + A_1^- + A_2^+ + 6A_2^- + 7A_3^+ + 7A_3^-. \tag{2}$$

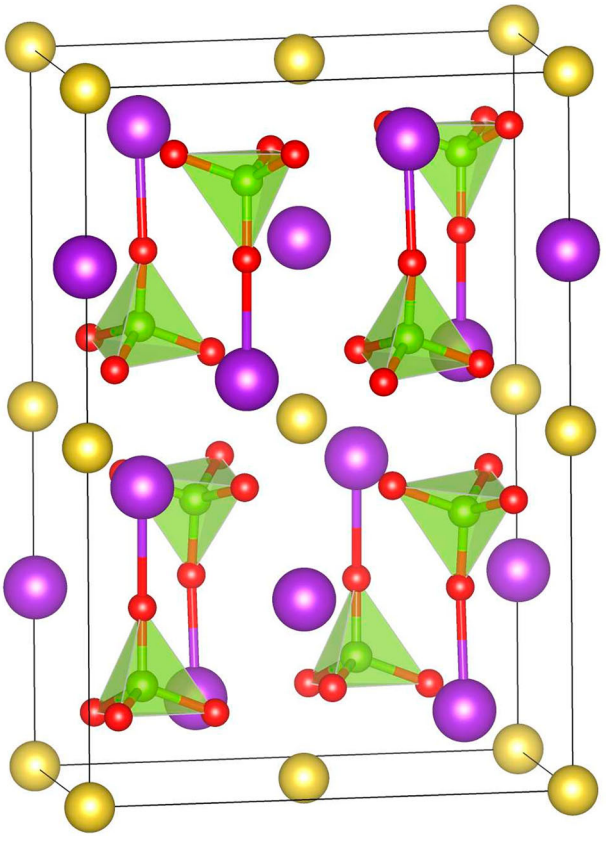

Figure 2. (color online) Crystal structure of the monoclinic (*C2/c)* phase of $K_3Na(SeO_4)_2$. Large (dark violet) filled atoms are potassium ones, opened (yellow) atoms are sodium ones, oxygen atoms are at the corners of tetrahedrae with selenium atoms at the tetrahedrae centers.

Table 2. Phonon symmetry in the trigonal phase of $K_3Na(SeO_4)_2$: space group $P\bar{3}m1$ (No. 164).

Atoms	*q*	*β*	Γ (000) $\bar{3}m$	A (0 0 ½) $\bar{3}m$	M (½ 0 0) 2/*m*	K (⅓ ⅓ 0) 32	L (½ 0 ½) 2*m*
Na	1a	$a_{2u}(z)$	2^-	2^-	2^-	2	2^-
	(000)	$e_u(x,y)$	3^-	3^-	1^-, 2^-	3	1^-, 2^-
	$\bar{3}m$						
K2	1b	$a_{2u}(z)$	2^-	1^+	2^-	2	1^+
	(0 0 ½)	$e_u(x,y)$	3^-	3^+	1^-, 2^-	3	1^+,2^+
	$\bar{3}m$						
K1	2d	$a_1(z)$	1^+,2^-	1^+,2^-	1^+,2^-	3	1^+,2^-
Se	(1/3 2/3 z)	e(x,y)	3^+,3^-	3^+,3^-	1^+,1^-, 2^+,2^-	1,2,3	1^+,1^-, 2^+,2^-
O1	3*m*						
O2	6i	a′(x;z)	1^+,2^-,3^+,3^-	1^+,2^-,3^+,3^-	1^+,1^+, 1^-,2^+,2^-, 2^-	1,2,3,3	1^+,1^+, 1^-,2^+,2^-, 2^-
	(x$\bar{x}$z)	a″(y)	1^-,2^+,3^+,3^-	1^+,2^-,3^+,3^-	1^+,1^-, 1^-,2^+,2^+, 2^-	1,2,3,3	1^+,1^-, 1^-,2^+,2^+, 2^-
	.m.						

The vibrational representation at the Γ-point of the BZ of the monoclinic phase C2/*c* is

$$\begin{aligned}\Gamma_{\text{opt}} + \Gamma_{\text{ac}} &= 19\Gamma_1^+ + 22\Gamma_1^- + 20\Gamma_2^+ + 23\Gamma_2^- = 19A_g + 22A_u + 20B_g + 23B_u,\\ \Gamma_{\text{ac}} &= \Gamma_1^- + 2\Gamma_2^- = A_u + 2B_u,\end{aligned} \tag{3}$$

Table 3. Phonon symmetry in the monoclinic phase of $K_3Na(SeO_4)$: space group *C2/c* (No. 15).

Atoms	*q*	*β*	Γ (000) 2/*m*	Y (½ ½ 0) 2/*m*	A (0 0 ½) 2/*m*	M (½ ½ ½) 2/*m*	V (½ 0 0) $\bar{1}$	L (½ 0 ½) $\bar{1}$
Na	4a (000) $\bar{1}$	a_u(x;y;z)	1^-, 2^-	1^-, 2^-	1	1	1^-, 1^-	1^+, 1^-
K2	4e (0y¼) .2.	a(y) b(x;z)	1^+, 1^- 2^+, 2^-	1^+, 1^- 2^+, 2^-	1 1	1 1	1^+, 1^- 1^+, 1^-	1^+, 1^- 1^+, 1^-
K1 Se O1 O2 O3 O4	8f (xyz) 1	a(x;y;z)	1^+,1^-,2^+,2^-	1^+,1^-,2^+,2^-	1,1	1,1	1^+,1^+,1^-,1^-	1^+,1^+,1^-,1^-

Table 4. Experimental and calculated structure parameters of the trigonal phase $P\bar{3}m1$ of $K_3Na(SeO_4)_2$.

Parameters	Experiment [1]	PBE
a, Å	5.906	5.98064
c, Å	7.552	7.67835
z, Se (2d)	0.27241	0.27467
z, K1 (2d)	0.8240	0.82920
z, O1 (2d)	0.4852	0.48982
x,z; O2 (6i)	0.1842, 0.1965	0.18187, 0.19660
E_g, eV	no data	3.6

with A_g and B_g modes being active in Raman spectra while A_u and B_u modes being active in infrared spectra. The non-zero Raman tensor components for A_g modes are diagonal elements α_{xx}, α_{yy}, α_{zz}, and α_{xy} while the B_g modes components are α_{xz}, α_{yz}.

4. *Ab initio* calculation results

The results of the $K_3Na(SeO_4)_2$ structure optimization compared to experimental data are reported in Table 4.

The atomic positions are given in fractional coordinates. For atoms occupying the Wyckoff positions (WP) 2d, two coordinates are fixed by symmetry and only one component *z* (along the **c** axis) is free. For atoms in the WP 6i, one coordinate is fixed while two others *x*, *z* (along the **a** (**b**) and **c** axes) are relaxed. For atoms in 1b (K2) and 1a (Na) positions, all coordinates are fixed by symmetry.

The *ab initio* calculations show a slight overestimation of the lattice parameters, with such effect being usually observed in calculations with the GGA-type functionals. The calculated phonon frequencies of the high-temperature trigonal phase $P\bar{3}m1$ compared with experimental data are given in Table 5.

The high-frequency modes are internal vibrations of Se-O_4 complexes. The A_{1g} vibration (883.95 cm^{-1}) is an in-phase stretching one along the **c**-axis connecting K1-Se atoms (see Figure 3 (a)) of both Se-O1-O2 units, while the A_{2u} (878.01 cm^{-1}) vibration is an antiphase one. The E_u mode (814.69 cm^{-1}) is a doubly degenerate antisymmetric stretching Se-O2 vibration (Figure 3(b)), the A_{2u} mode (812.1 cm^{-1}) is an antiphase symmetric stretching vibration involving oxygen atoms in a tetrahedron, while A_{1g} (806.2 cm^{-1}) is the in-phase one. The A_{1g} mode (806.2 cm^{-1}) is a bending vibration (Figure 3(c)). For the other low-frequency range, only Raman-active modes will be discussed. The A_{1g} mode (404.82 cm^{-1}) is a stretching mode of oxygen tetrahedron forming the Se-

Table 5. Calculated and experimental (in parentheses) phonon frequencies of the trigonal $P\bar{3}m1$ phase of $K_3Na(SeO_4)_2$

	Calculated and experimental [4] phonon frequencies, cm^{-1}					
N	A_{1g}	E_g	A_{2u}	E_u	A_{1u}	A_{2g}
1				32.29		
2		39.02 (60)				
3						68.44
4					86.07	
5				88.35		
6		94.61 (106)				
7	98.1 (89)					
8				106.24		
9			107.37			
10		114.52 (137)				
11			137.77			
12	141.55 (162)					
13				167.28		
14			189.17			
15				301.76		
16		307.56 (344)				
17				373.34		
18			375.86			
19		381.06 (420)				
20	404.82 (442)					
21		804.95 (862)				
22	806.2 (853)					
23			812.1			
24				814.69		
25			878.01			
26	883.95 (931)					

O_4 complex (Figure 4(a)), the E_g mode (381.06 cm^{-1}) is a rotational mode of oxygens O2 with the translation of Se and O1 atoms (Figure 4(b)). The E_g mode (307.56 cm^{-1}) is a complex vibration involving a rotation of two O2 atoms while the third O2 atom moves away from O1 (Figure 4(c)). The A_{1g} mode (141.55 cm^{-1}) is a simple stretching vibration, in which the Se-O_4 complex and potassium K1 atoms move towards along the **c**-axis. The low-frequency E_g mode (114.52 cm^{-1}) is a stretching vibration of two complexes K-Se-O_4 moving towards perpendicular to the **c**-axis in the unit cell. The A_{1g} mode (98.1 cm^{-1}) is a bending vibration with two K-Se-O_4 units moving in opposite direction along the **c**-axis. The E_g mode (94.61 cm^{-1}) is a complex vibration of K-Se-O_4 unit, with rotation of two O2 atoms while the third oxygen atom O2 is fixed, the Se and O1 atoms moving away from potassium K1 atom along **a** or **b** axis (Figure 4(d)). The lowest frequency E_g mode (39.02 cm^{-1}) is a vibration of a whole K-Se-O_4 unit.

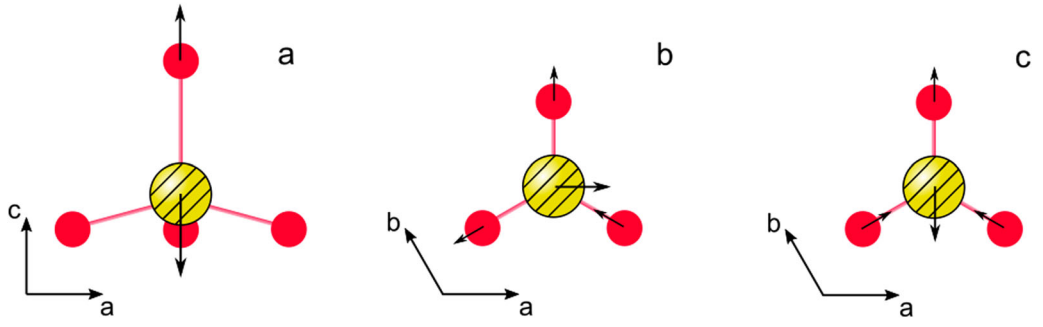

Figure 3. (color online) Displacements of atoms in the internal vibrations of the trigonal phase of $K_3Na(SeO_4)_2$. Filled (red) circles are the oxygen atoms, large (yellow) dashed circles are the selenium atoms.

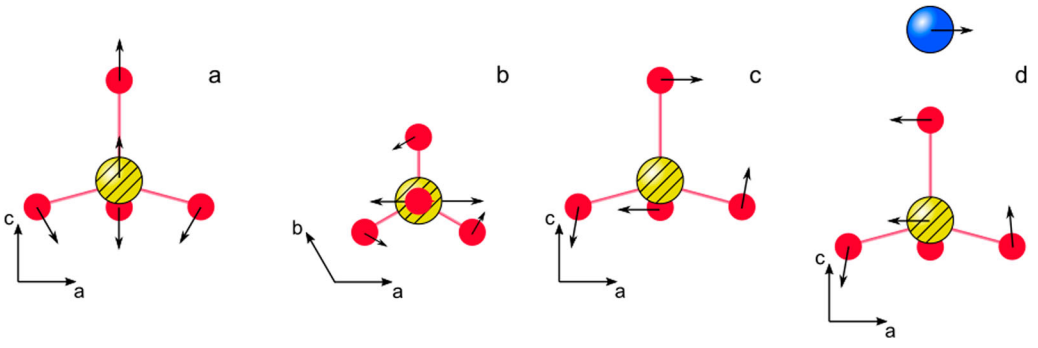

Figure 4. (color online) Displacements of atoms in the low-frequency range. Filled (red) circles are the oxygen atoms, large yellow (hatched) circles are the selenium atoms, large (blue) circles are the potassium atoms K1.

The calculated phonon spectra do not reveal imaginary frequencies in the BZ centre (Γ-point) of the $K_3Na(SeO_4)_2$ trigonal phase. Thus, the *ab initio* approach does not predict the existence of soft modes at the Γ-point of BZ. We have studied the phonon band structure (Figure 5) within the whole BZ along high-symmetry directions by the supercell approach, with calculating of force constants using the finite displacement method [20]. The most noticeable feature in phonon dispersion curves is the existence of the A_3^+ phonon with an imaginary frequency at the BZ boundary (see Section 3). The A_3^+ mode is a double-degenerate vibration which originates from the transverse acoustic branch and the optical phonon E_u (with the frequency 32.29 cm^{-1} at the Γ-point) due to anticrossing of these branches in the Γ-point vicinity along the Γ-A direction (see Figure 5). The imaginary frequency of this mode indicates its softening.

The mode is a rotationally translational vibration, which involves the rotations of SeO_4 tetrahedra as well as the potassium (K1, K2) and selenium atom displacements along the **a** or **b** axis (Figure 6). An imaginary value of the soft-mode frequency indicates that the crystal is in the high-symmetry

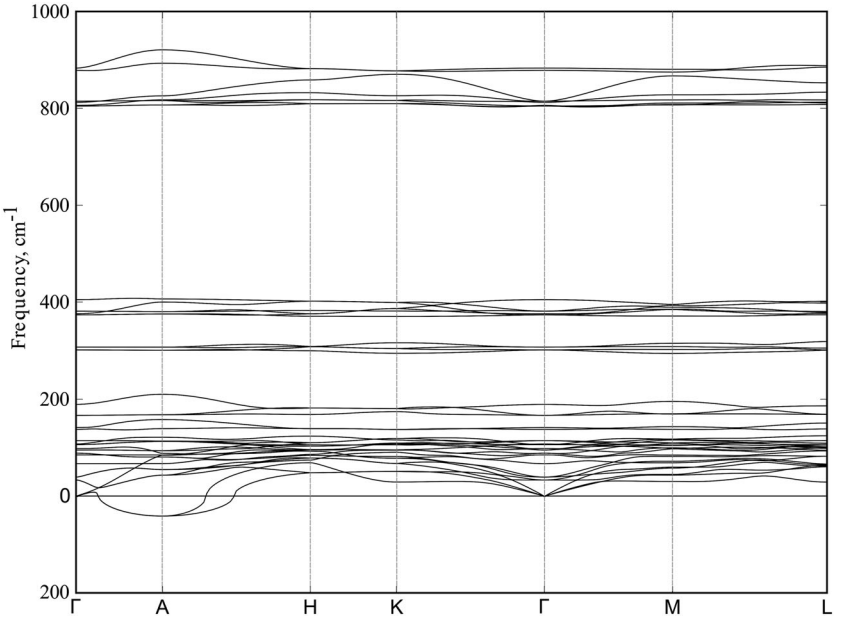

Figure 5. Phonon dispersion curves of the trigonal phase of $Ka_3Na(SeO_4)_2$.

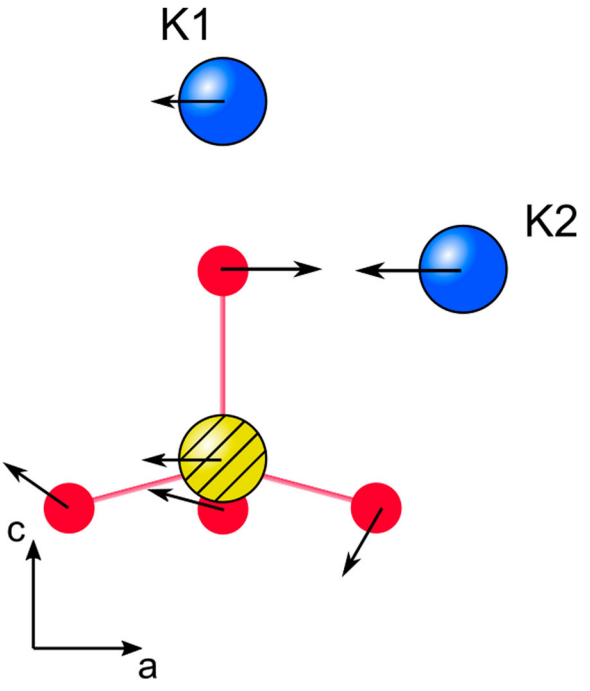

Figure 6. (color online) Displacements of atoms in primitive cell within soft-mode vibration. The full atom displacements corresponds to antiphase displacements of atoms in doubled cell. Small filled (red) circles are oxygen atoms, large dashed (yellow) circles are selenium atoms, large filled (blue) atoms is potassium atoms K1.

metastable phase. Hence, the atomic displacements generating this mode should lead to the global minimum (low-temperature phase). Since the soft mode is the double-degenerate one, it could lead to two different low-symmetry phases. In fact, this is the case with one mode being responsible for the transition to the low-symmetry monoclinic phase with space group *C2/m* while the other to the *C2/c* phase (both with doubling the unit cell). Each phase is characterized by its proper energy. The monoclinic phase *C2/m* corresponds to a minimum at $E_{\text{total}} = -141.917714$ eV, while the minimum for monoclinic phase *C2/c* is $\underline{E}_{\text{total}} = -141.914746$ eV. Therefore, the *C2/c* space group is a more stable one. It should be stressed that the *C2/m* phase found in these calculations does not coincide with the intermediate *C2/m* phase predicted by group theory in Section 5 (Figure 8). The latter was predicted as a result of a spontaneous elastic strain with conservation of the number of atoms in the primitive cell whereas as the former is a result of softening of the double-degenerated zone-edge phonon A_3^+.

The difference in total energy is $\Delta E = 141.917714 - 141.914746 = 2.97$ meV. This corresponds to the temperature range $\Delta T^{\text{theor}} = T_{c1} - T_{c2} = 34.44$ K of coexistence of both monoclinic phases *C2/m* and *C2/c*. This value depends negligibly on increasing the size of the basis set. The increase of the E_{cut} value by 50 eV results to the difference in energy $\Delta E = 2.89$ meV, thus the calculations accuracy of $\Delta T^{\text{theor}} \sim 1$ K. For $T < T_{c2}$, only one phase *C2/c* is stable, which follows from the energy minimum condition. This is in a good agreement with the experimental data [3] where the temperature range of monoclinic phase coexistence is found to be $T_{c1} - T_{c2} = 346$ K–329 K = 17 K and the low-temperature monoclinic phase below T_{c2} has been found to be *C2/c*. The lattice parameters and atomic positions of the monoclinic phase *C2/c* compared with experimental data are reported in the Table 6. The sodium atom Na1 is fixed by symmetry (WP 4a), the potassium atom K2 (WP 4e) has only one free coordinate *y*, other atoms occupy general WP's 8f with three free coordinates (see Table 3).

The phase transition to the monoclinic phase is accompanied by spontaneous strain and the formation of ferroelastic domains in the crystal [2]. The ferroelastic domain structure was observed in

Table 6. Experimental and calculated structure parameters of the monoclinic *C2/c* phase of $K_3Na(SeO_4)_2$.

Parameter	Experiment [1]	Calculations, this work
a, Å	10.162	10.369
b, Å	5.867	5.979
c, Å	15.021	15.415
β,^{o}	90	89.884
x,y,z; Se1 (8f)	0.166, 0.492, 0.137	0.164, 0.486, 0.133
x,y,z; K1(8f)	0.168, 0.489, 0.413	0.170, 0.477, 0.406
y, K2(4e)	0.9733	0.952
x,y,z; O1(8f)	0.171, 0.527, 0.243	0.167, 0.562, 0.237
x,y,z; O2(8f)	0.09, 0.707, 0.089	0.089, 0.686, 0.076
x,y,z; O3(8f)	0.0896, 0.258, 0.109	0.085, 0.244, 0.118
x,y,z; O4(8f)	0.315, 0.482, 0.097	0.315, 0.460, 0.095

Table 7. Calculated and experimental (in parentheses) phonon frequencies of the monoclinic *C2/c* phase of $K_3Na(SeO_4)_2$.

A_g	B_g
43.64 (36)	28.67 (28)
45.44 (61)	66.58 (60)
56.3 (65)	78.03 (71)
97.89 (97)	88.28 (99)
111.47 (110)	119.63 (125)
112.39 (129)	136.77 (136)
119.34 (136)	151.38 (153)
123.89 (143)	317.36 (346)
146.41 (173)	807.6 (853)
379.55 (339)	816.32 (862)
384.6 (418)	897.1 (869)
403.84 (444)	
808.14 (853)	
871.13 (862)	

the (001) plane. Three types of domain orientations are observed. Thus, it is not possible to separate the Raman-tensor components α_{xz} and α_{yz} in the experimental spectra unless the sample is not a single-domain one. Only *xy* polarization spectra allow one to detect unambiguously the B_g modes. The phonon frequencies of the monoclinic *C2/c* phase compared with the experimental ones are given in Table 7.

The experimental data in the paper [4] do not provide the low-temperature *zz*-polarized Raman spectra in the middle- and high-frequency range. Hence, for some modes the symmetry cannot be detected explicitly. In Table 7, only those modes are reported which unambiguously observed in the experiment.

5. Discussion

The displacive phase transitions in solids can be also analyzed using the programs and retrieval tools of the BCS. The symmetry analysis of phase transitions in $K_3Na(SeO_4)_2$ crystals has been performed using the AMPLIMODES program [24,25] which allows one to determine the global structural distortion that relates high and low-symmetry phases. Based on the experimentally determined structure data, it determines also the primary and secondary symmetry modes compatible with the determined sequence of phase transitions and calculates the amplitudes of different symmetry-adapted distortions presented in the low-symmetry phase as well as their polarization vectors.

The screenshots from the AMPLIMODES program are given in Figures 7 and 8.

Symmetry Modes Summary

Atoms	WP	Modes
O2	6*i*	GM1+(2) GM3+(3) A2+(1) **A3+(3)**
O1 Se1 K1	2*d*	GM1+(1) GM3+(1) **A3+(1)**
K2	1*b*	**A3+(1)**

Note: The primary mode is written in bold letters

Figure 7. Screenshot from the AMPLIMODES program which shows the primary (in bold letters) and secondary modes which drive the trigonal-monoclinic transition and the atoms in the unit cell which contribute to these modes.

K-vector	Irrep	Direction	Isotropy Subgroup	Dimension	Amplitude (Å)
(0,0,0)	GM1+	(a)	P-3m1 (164)	5	0.0353
(0,0,0)	GM3+	(-0.500a,0.866a)	C2/m (12)	6	0.0889
(0,0,1/2)	A2+	(a)	P-3c1 (165)	1	0.0089
(0,0,1/2)	A3+	(-0.866a,-0.500a)	C2/c (15)	7	0.4888

Global distortion: 0.4982 Å

Figure 8. Screenshot from the AMPLIMODES program which shows the amplitudes of the distortions connected with primary and secondary modes.

From Figures 7 and 8, one can see that the AMPLIMODE program [24,25] gives three possible scenario of phase transition sequences.

The first one is the direct transition $P\bar{3}m1 \rightarrow C2/c$ driven by one primary mode A_3^+ and two secondary modes A_2^+ and Γ_3^+. This scenario can be verified by experiments because the zone-edge soft phonon A_3^+ transforms into a pair of $\Gamma_1^+ + \Gamma_2^+$ phonons in the low-symmetry phase as determined by the CORREL program of BCS [10]. The transformation matrix relating the unit cells of the initial trigonal $P\bar{3}m1$ and final monoclinic $C2/m$ phases is

$$\begin{pmatrix} -1 & -1 & 0 \\ 1 & -1 & 0 \\ 0 & 0 & 2 \end{pmatrix}. \tag{4}$$

The second and third scenarios are transitions *via* intermediate phases, either $P\bar{3}c1$ or $C2/m$, respectively. However, the Γ_3^+ distortions (0.0889 Å) connected with the transition into the monoclinic intermediate phase $C2/m$ are 10 times larger than those connected with the transition into the trigonal intermediate phase $P\bar{3}c1$ (0.0089 Å). Therefore, the latter one can be neglected and excluded from group theoretical analysis. The distortion with the Γ_3^+ symmetry, which is responsible for the transition into the monoclinic intermediate phase $C2/m$, gives an essential contribution into the global distortion (0.4982 Å), though much smaller than the primary A_3^+ mode (0.4888 Å). (Note, that there is a phonon as well as spontanious strain with the Γ_3^+ symmetry.) Thus, the group theoretical analysis is in a good agreement with *ab initio* calculations.

6. Conclusion

Several words should be added about the microscopic nature of the order parameter. Since the discussed phase transition is the improper ferroelastic one [26], the spontaneous elastic strain is not a primary order parameter. However, our a*b initio* calculations show the unit K1-SeO_4 distorts and looses C_3 axis (see Figure 6). The nearest-to-potassium K1 oxygen atom O1 shifts to potassium K2 atom which results that K1, O1, and Se atoms are no longer lie in the line. Thus, the angle

$\phi = \angle$ (K2 O1 Se) is no longer equal to 180°, which leads to the trigonal symmetry break. While increasing pressure (which is a simulation of lowering temperature), the *ab initio* calculations predict the decrease of this angle. Thus, we suppose the microscopic nature of the order parameter is the shift of the K1-SeO_4 unit mass center. The mass center lies at the C_3 axis in the paraphase and monotonically shifts in the ferrophase that leads to order parameter increase.

Summing up, among three possible scenarios of the phase transition from the high-symmetry trigonal $P\bar{3}m1$ to the low-symmetry monoclinic phase *C2/c* in the $K_3Na(SeO_4)_2$ crystals the third one *via* a mixture of two monoclinic phases *C2/m* and *C2/c* (both with the unit cell doubling) is realized. It is driven by the zone-edge soft phonon which symmetry is described by two-dimensional irreducible representation A_3^+. Depending on the direction of the order parameter A_3^+ could induce a transition either into *C2/m* or *C2/c*.

Disclosure statement

No potential conflict of interest was reported by the author(s).

ORCID

Yu. E. Kitaev http://orcid.org/0000-0003-4188-7384
E. M. Roginskii http://orcid.org/0000-0002-5627-5877
V. S. Zhandun http://orcid.org/0000-0003-0744-4205

References

[1] Fábry J, Breczewski T, Petriček V. Structure determination of the ferroelastic triple-twinned phase of $K_3Na(SeO_4)_2$ at 291 K and its parent phase at 390 K. Acta Crystallogr B. 1993;49:826–832.
[2] Krajewski T, Piskunowicz P, Mróz B. Structural phase transitions in $K_3Na(SeO_4)_2$ crystals. Phys Status Solidi (a). 1993;135:557–564.
[3] Diaz-Hernández J, Mañes JL, Tello MJ, et al. Ferroelastic phase transitions in the $K_3Na(SeO_4)_2$ glaserit-type crystal. Phys Rev B. 1996;53:14097–14102.
[4] Kaczmarski M, Mróz B. Raman study of the ferroelastic phase transition in $K_3Na(SeO_4)_2$. Phys Rev B. 1998;57:13589–13598.
[5] Kaczmarski M, Eichner A, Mielcarek S, et al. Ir temperature study of internal vibrations in $K_3Na(SeO_4)_2$. Vib Spectrosc. 2000;23:77–81.
[6] Lim AR. A nuclear magnetic resonance study of the ferroelastic phase transitions of $K_3Na(CrO_4)_2$ and $K_3Na(SeO_4)_2$ single crystals. J Phys: Condens Matter. 2008;20:135212-1-7.
[7] Kitaev YE, Maksimova TI, Hermanowicz K, et al. Observation of an intermediate phase in the $K_3Na(CrO_4)_2$ ferroelastic by Raman scattering. Phys Solid State. 2012;54:134–139.
[8] Kitaev YE, Maksimova TI, Hermanowicz K, et al. Temperature dependence of IR absorption spectra of the $K_3Na(CrO_4)_2$ ferroelastic. Phys Solid State. 2013;55:145–149.
[9] Kitaev YE, Maksimova TI, Hermanowicz K, et al. Manifestation of an intermediate phase in a ferroelastic $K_3Na(CrO4)_2$:MnO42− in Raman and IR absorption spectra. Opt Spectrosc. 2014;116:858–863.
[10] Aroyo MI, Kirov A, Capillas C, et al. Bilbao crystallographic server II: representations of crystallographic point groups and space groups. Acta Crystallogr A. 2006;62:115–128. Available from: www.cryst.ehu.es
[11] Aroyo MI, Perez-Mato JM, Capillas C, et al. Bilbao crystallographic server I: databases and crystallographic computing programs. Z. Kristallogr. 2006;221:15–27.
[12] Aroyo MI, Perez-Mato JM, Orobengoa D, et al. Crystallography online: bilbao crystallographic server. Bulg Chem Commun. 2011;43:183–197.
[13] Kresse G, Hafner J. Ab initio molecular-dynamics simulation of the liquid-metal-amorphous-semiconductor transition in germanium. Phys Rev B. 1994;49:14251–14269.
[14] Kresse G, Furthmüller J. Efficiency of ab-initio total energy calculations for metals and semiconductors using a plane-wave basis set. Comput Mater Sci. 1996;6:15–50.
[15] Perdew JP, Burke K, Ernzerhof M. Generalized gradient approximation made simple. Phys Rev Lett. 1996;77:3865–3868.
[16] Blöchl PE. Projector augmented-wave method. Phys Rev B. 1994;50:17953–17979.
[17] Kresse G, Joubert D. From ultrasoft pseudopotentials to the projector augmented-wave method. Phys Rev B. 1999;59:1758–1775.

[18] Murnaghan FD. The compressibility of media under extreme pressures. Proc Natl Acad Sci USA. 1944;30:244–247.
[19] Monkhorst HJ, Pack JD. Special points for Brillouin-Zone integrations. Phys Rev B. 1976;13:5188–5192.
[20] Togo A, Tanaka I. First principles phonon calculations in materials science. Scr Mater. 2015;108:1–5.
[21] Smirnov MB, Roginskii EM, Kazimirov V, et al. Spectroscopic and computational study of structural changes in γ-LiV_2O_5 cathodic material induced by lithium intercalation. J Phys Chem C. 2015;119:20801–20809.
[22] Cracknell AP, Davies BL, Miller SC, et al. Kronecker product tables. Vol. 1. General introduction and tables of irreducible representations of space groups. New York (NY): IFI/Plenum; 1979.
[23] Bradley CJ, Cracknell AP. The mathematical theory of symmetry in solids. Clarendon: Oxford; 1972.
[24] Orobengoa D, Capillas C, Aroyo MI, et al. Amplimodes: symmetry-mode analysis on the Bilbao crystallographic server. J Appl Cryst. 2009;42:820–833.
[25] Perez-Mato JM, Orobengoa D, Aroyo MI. Mode crystallography of distorted structures. Acta Cryst A. 2010;66:558–590.
[26] Stokes HT, Hatch DM. Isotropy subgroups of the 230 crystallographic space groups. Singapore: Singapore: World Scientific; 1988.